Environmental Science Nano

PAPER

View Article Online
View Journal | View Issue

Cite this: *Environ. Sci.: Nano*, 2019, **6**, 3349

Single-particle ICP-TOFMS with online microdroplet calibration for the simultaneous quantification of diverse nanoparticles in complex matrices†

Kamyar Mehrabi, [a] Detlef Günther[a] and Alexander Gundlach-Graham *[ab]

Inductively coupled plasma time-of-flight mass spectrometry (ICP-TOFMS) is unique in its ability to provide multidimensional information about nanoparticles (NPs) including multi-element composition, size/mass distribution, and number concentration. We present an online and matrix-matched calibration method for the multiplexed analysis of NPs using ICP-TOFMS. In our system, NP mass is determined based on absolute sensitivities measured with microdroplet standards. Because we introduce microdroplets along with NP-containing samples, they provide matrix-matched calibration of element mass. For accurate determination of particle number concentration (PNC), we spike a plasma-uptake standard element, *e.g.* Cs, into NP containing samples and then—based on absolute sensitivity from microdroplet signals—can directly determine the sample uptake rate into the plasma. Our online microdroplet method requires no external NP standards and a detailed explanation of the approach is provided. As a proof-of-principle, we applied this approach for the quantification of well-characterized engineered NPs (Ag, Pt, and Au NPs) in different matrices, including phosphate-buffered saline, triton-x surfactant, and effluent from a waste water treatment plant (WWTP). Results demonstrate accurate multiplexed quantification of spiked NPs in all matrices in terms of both element mass and PNC, which suggests the utility of the approach for quantification of NPs in challenging or not well-defined environmental matrices. For the WWTP effluent sample, endogenous NPs and spiked NPs are quantified in a single run.

Received 3rd June 2019,
Accepted 1st October 2019

DOI: 10.1039/c9en00620f

rsc.li/es-nano

Environmental significance

Description and quantification of anthropogenic (both engineered and incidental) nanoparticles (NPs) in environmental compartments continues to be a limiting factor for risk assessment and the development of NP pollution monitoring approaches. Here, we describe an online calibration method for single-particle inductively coupled plasma time-of-flight mass spectrometry (sp-ICP-TOFMS) that offers matrix-independent quantification of metal- and metal-oxide nanoparticles in terms of element mass and particle number concentration (PNC). sp-ICP-TOFMS combined with online microdroplet calibration provides a route toward high-throughput and accurate measurements of diverse NP types *in situ* from aquatic environments. For example, with our online microdroplet calibration method, measurements of NPs in matrices with high salt or dissolved organic content (DOC) can be accurately made without any *a priori* knowledge about matrix composition or additional matrix compensation strategies. The comprehensive description of NP compositions and concentrations now measurable by sp-ICP-TOFMS will support progress in the development of NP technologies and regulations.

Introduction

Widespread use of nanoparticles (NPs) and incidental production anthropogenic NPs continues to increase the risk of NP emission into environmental and biological systems.[1–5] Better characterization and quantification of NPs *in situ*, *i.e.* in these complex matrices, requires robust and high-throughput measurements.[6,7] Single-particle (sp)-ICP-TOFMS is a promising approach that enables multiplexed detection and quantification of diverse metal and metal-oxide NPs.[8–11] To date, ICP-TOFMS is the only ICP-MS-based method that allows for quantitative untargeted multi-element measurements from individual particles. Especially for aquatic environmental samples, sp-ICP-MS offers the potential to measure environmentally relevant particle number concentrations (PNCs) (10^2–10^6 NPs mL^{-1}), even in the presence of high dissolved element backgrounds.[12] This characteristic makes sp-ICP-MS well suited to be used to quantify anthropogenic

[a] *ETH Zurich, Department of Chemistry and Applied Biosciences, Laboratory of Inorganic Chemistry, Vladimir-Prelog-Weg 1, 8093 Zurich, Switzerland*
[b] *Iowa State University, Department of Chemistry, 2415 Osborn Drive, Ames, IA 50011, USA. E-mail: alexgg@iastate.edu*

† Electronic supplementary information (ESI) available. See DOI: 10.1039/c9en00620f

NP pollution locally and globally, which is critical for accurate (eco-) toxicological risk assessments of many NP types.[13–18] However, the trueness of NP counting and sizing by sp-ICP-MS depends on how accurately the sample uptake into the ICP (*i.e.* transport efficiency) and signal per analyzed unit of mass (*i.e.* sensitivity) are determined.[19–21] Depending on the NP-containing matrix, both transport efficiency and/or elemental sensitivity may change and cause inaccurate calibration of PNC or element mass.[22] In the context of environmental analysis, temporally and spatially variable matrix characteristics, such as dissolved organic content, total salt content, or pH, could impact the accuracy of sp-ICP-MS analysis. Our online approach for quantification of NPs by sp-ICP-MS is designed to overcome matrix effects through direct compensation for matrix-dependent signal attenuations or enhancements.

The most common approach to calibrate NP mass (m_p) with sp-ICP-MS is based on the particle-size method first reported by Pace *et al.*[19] In this method, a suspension of well-characterized mono-disperse NPs (such as NIST RM8013, 56 nm diameter Au NPs) is analyzed by sp-ICP-MS to measure ion counts per NP (I_p) and absolute sensitivity per NP ($S_{NP,std}$) in counts g^{-1}. A calibration curve using a standard solution of the same analyte as the NPs is also measured to determine a concentration-based sensitivity ($S_{neb,std}$, counts s^{-1} per g mL^{-1}). Assuming the instrument response function (counts g^{-1}) is equal for particles and dissolved analyte, then the sample flux into the plasma (q_{plasma}, mL s^{-1}) can be determined as shown in eqn (1). Additionally, if the sample flow rate (q_{neb}, mL s^{-1}) into the nebulizer is measured along with standard solutions, then the transport efficiency (η_{neb}) can be calculated; see eqn (2). To calibrate NPs with element composition different than the NP standard, the transport efficiency is used to calculate the total mass of any analyte standard (i) introduced into the plasma during the NP measurement time, t_p, *e.g.* the dwell time. In this way, the absolute element sensitivities can be determined, which allows the mass of the element to be determined in analyte NPs; see eqn (3). While the particle-size method has been applied many times in sp-ICP-MS studies, it has a number of drawbacks, which include the required use of NP standards, dependency on a stable η_{neb} for accurate size and PNC calibration, and no direct compensation for matrix effects.[22]

$$q_{plasma} = \frac{S_{neb,std}}{S_{NP,std}} \quad (1)$$

$$\eta_{neb} = \frac{q_{plasma}}{q_{neb}} \quad (2)$$

$$m_{p,i} = \frac{(I_{p,i} - I_{bkgd,i}) \times \eta_{neb}}{t_p \times S_{neb,i}} \quad (3)$$

Recently, several research groups have developed methods to determine element mass of individual NPs without having to measure transport efficiency and the sensitivity of dissolved calibration standards. One approach is to use monodisperse microdroplets as a proxy for NP standards.[23–25] Here, the size of uniform microdroplets is measured online and, based on known concentrations of element(s) of interest, the average signals from discrete microdroplets serve as single-point sensitivity factors (counts/mass of analyte) that can be used to determine element mass in NPs.[8,24,25] Alternatively, other researchers have used isotope dilution analysis (IDA)[26] and internal standard (ISD)[27] approaches. IDA in sp-ICP-MS is limited by low signals from single particles, which do not typically allow for precise isotope ratios and is only suitable for NPs composed of elements with more than one isotope (such as silver) and for which there exists a readily available isotopically enriched standard. ISD is most often used to correct for sensitivity drift during ICP-MS analysis, though selection of a suitable ISD could also help correct for matrix effects. Similar to ISD, the use of a multi-nebulizer, in which sample is introduced from one nebulizer and internal standard solution from another nebulizer into the same spray chamber, allows for specific correction of plasma-based matrix effects;[28] however, sample-introduction-related matrix effects that control transport efficiency into the plasma remain a challenge.

Here, we present an online microdroplet calibration strategy to size and count NPs—and account for plasma-related and sample-introduction related matrix effects—in a single step. We use a dual-sample introduction approach in which individual microdroplets that contain known element concentrations are merged into the aerosol generated by a pneumatic nebulizer, and introduced into the ICP.[29] The online microdroplet approach provides automatic matrix-matched calibration of signals from individual NPs.[30,31] Additionally, we spike a known concentration of an plasma-uptake standard (*e.g.* cesium, Cs) into the NP-containing samples and the microdroplet standards. Through detection of the nebulized and microdroplet-contained Cs, we are able to determine sample uptake rates into the plasma (q_{plasma}) for every sample and directly calculate PNCs. This new method enables us to further investigate the effects that sample matrices can have on measured particle size and PNC. Online microdroplet calibration provides a direct approach for the multiplexed quantification of multiple NP types in a single measurement run, both in terms of $m_{p,i}$ and PNC; we demonstrate this multi-NP and multi-element quantification through analysis of waste water treatment plant (WWTP) effluent.

Materials and methods

Chemicals

Suspensions of monodisperse Au (Ø = 10 3 ± 10 nm), Au (49.9 ± 2.2 nm), Pt (72 ± 4 nm), and Ag (79 ± 7 nm) NPs (99.99% purity) in 2 mM aqueous diluted sodium citrate, with PNCs of 4.7×10^9, 4.2×10^{10}, 1.3×10^{10} and 7.6×10^9 particles/mL, were purchased from nanoComposix (San Diego, CA, USA). Prior to analysis, NP suspensions were diluted in ultrapure water (>18 MΩ cm^{-1}). PBS 1× (pH 7.4, Gibco, Thermofisher Scientific, USA) and Triton X-114

(Merck, Germany) were diluted in ultrapure water for use as NP-containing matrices. The WWTP effluent sample was obtained from a plant in Dübendorf, Switzerland and stored at 4–5 °C for one day before analysis. Aqueous elemental standards and microdroplet solutions were prepared from 1000 mg L^{-1} single-element standard solutions (Inorganic Ventures, USA) in trace-grade 3% HCl (TraceSelect, Fluka Analytical, Switzerland) and sub-boiled 1% HNO_3. Dilutions were prepared gravimetrically using an analytical balance (Mettler AE240, Mettler-Toledo, Switzerland).

Instrument

The ICP-TOFMS instrument used in our work was manufactured by TOFWERK (Thun, Switzerland). We used the icpTOF-2R, which has a native mass resolving power ($m/\Delta m$ at FWHM) of ~6000 and an extraction frequency of 21.739 kHz. More details on the icpTOF instrument can be found elsewhere.[32,33] Specific operating conditions of the icpTOF for our experiments are provided Table S1.† Microdroplets were generated with a MD-E-3000 droplet dispenser (Microdrop Technologies GmbH, Germany) equipped with a 50 mm diameter Autodrop Pipette (AD-KH-501-L6). Droplets were introduced into a vertical falling tube filled with a helium/argon gas mixture to accelerate droplet desolvation.[25] Dried microdroplet residues were mixed with nebulized aerosols from a pneumatic nebulizer (MicroFlow, Element Scientific Inc., USA) and a baffled cyclonic spray chamber in a PFA T-piece (Swagelok, USA) before transport into the ICP; this configuration is based on dual inlet system of Ramkorun-Schmidt *et al.*[29] Fig. 1 is a schematic diagram of our online microdroplet calibration system. Each measurement starts and ends with a burst of 1000 microdroplets (droplet generation at 50 Hz for 20 s); between these microdroplet bursts is the single-NP detection region that was typically 150 s. Microdroplet bursts bracket the NP-detection region to check for signal intensity drift. No signal drift was observed in measurements described here; however, drift could be corrected through linear interpolation of sensitivities based on microdroplet standard bracketing.

Data analysis: online microdroplet calibration and sample uptake determination

As discussed in the introduction, our online microdroplet calibration system is used to simultaneously calibrate for NP mass ($m_{p,i}$) and particle-number concentration (PNC), by direct measurement of absolute element sensitivities of each analyte, i, ($S_{drop,i}$) and the sample uptake rate into the plasma (q_{plasma}). Importantly, this calibration approach does not require any external NP reference materials and, because both $S_{drop,i}$ and q_{plasma} are measured in the NP-containing matrices, can be used to compensate for matrix-dependent ion-signal yields in the plasma and for sample-transport effects.

Data analysis was performed in Matlab (verR2017b Mathworks, MA, USA). In our Matlab script, microdroplet signals were isolated from data traces by their multi-element fingerprints, and NPs were identified based on a critical value detection criterion (S_C) that gives a false-positive rate of 0.01%; critical values were based on modelling TOFMS signals as a compound Poisson signal distribution.[32,34] Prior to data analysis in Matlab, TOF spectra were mass calibrated in TOFWARE (ver. 2.5.11, TOFWERK, run in Igor-Pro 7 environment) and exported as .CSV time traces of counts *vs.* time for all analyte isotopes. Processed sp-ICP-TOFMS data were plotted with OriginPro (ver 8.6.0, OriginLab Corp., MA, USA) and

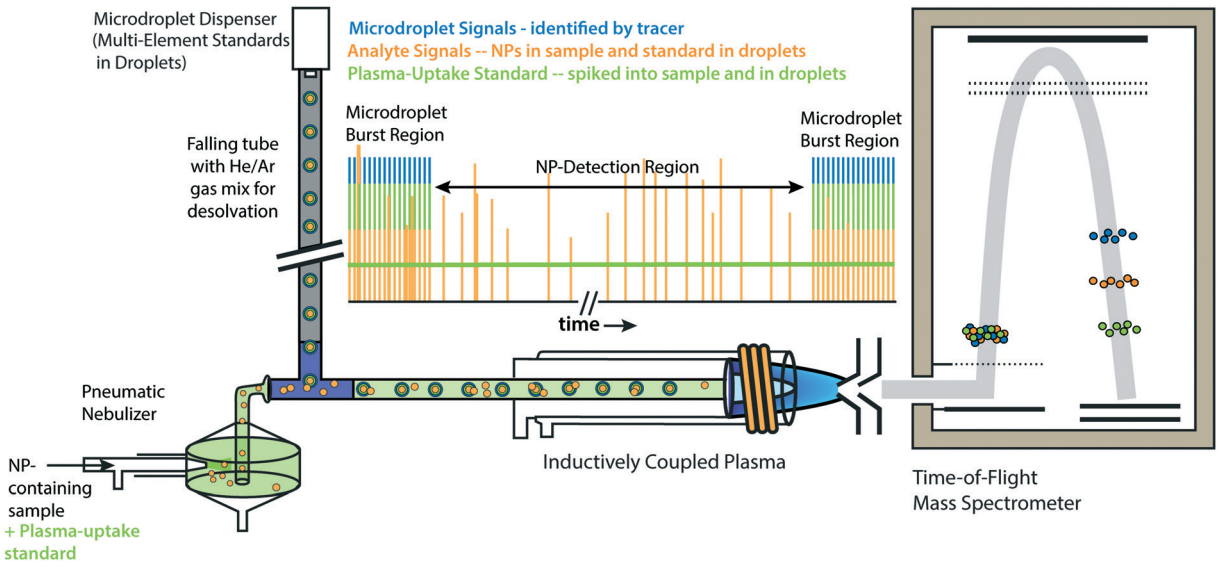

Fig. 1 Schematic of the dual sample introduction system for sp-ICP-TOFMS with online microdroplet calibration and online plasma-uptake measurements. Inserted graph: time trace of the element signals that are only present in a droplet (blue), present in the droplet and NP of interest (orange), and present from the plasma-uptake standard in both the nebulized sample and the microdroplets (green).

final figures were assembled in Adobe Illustrator (ver. 16.2.0, Adobe Systems Inc., USA).

Following isolation of microdroplet- and NP-based signals, eqn (4)–(10) were used to establish the online calibration of both $m_{p,i}$ and PNC. Calibration of $m_{p,i}$ depends only on the absolute mass sensitivity measured from the microdroplets ($S_{drop,i}$, counts g^{-1}) of each analyte element, i. $S_{drop,i}$ is determined for each sample analysis and is calculated as shown in eqn (4), where $I_{drop,i}$ (counts) is the average analyte intensity from individual calibrant microdroplets, $C_{drop,i}$ (g mL^{-1}) is the concentration of analyte i in the microdroplets, and V_{drop} (mL) is the measured average volume of the microdroplets. As seen in eqn (5), the mass of each element in single NPs ($m_{drop,i}$, g) introduced *via* the pneumatic nebulizer is simply the measured single-NP analyte signal ($I_{p,i}$) divided by the absolute mass sensitivity. Because microdroplet and NP signals all are measured in the same matrix, no background subtraction is required for element quantification. Effective NP diameter ($d_{eff,i}$, cm) is then calculated assuming NPs are round and have the bulk density (ρ) of analyte i (see eqn (6)).

PNC is calculated by dividing the frequency of NPs measured (f_{NP}) by the sample flow rate into the plasma (q_{plasma}). To determine q_{plasma}, the measured sensitivity for the nebulized plasma-uptake standard (*i.e.* Cs) was determined as shown in eqn (7), where $\lambda_{neb,Cs}$ is the average intensity in count s^{-1} for Cs measured within the "NP-detection region" of the experiment time trace (see Fig. 1). To determine the absolute mass sensitivity of Cs in microdroplets ($S_{drop,Cs}$), average Cs signal from nebulized sample ($I_{neb,Cs}$, counts) was subtracted from microdroplet-based Cs signal ($I_{drop,Cs}$, counts), and then divided by the mass of Cs in each microdroplet (see eqn (8)). Plasma-uptake rate was calculated with eqn (9), in which $S_{neb,Cs}$ (counts s^{-1} per g mL^{-1}) and $S_{drop,Cs}$ (counts g^{-1}) are the concentration-based and absolute sensitivities for Cs. The calculation q_{plasma} assumes that the Cs concentration into the plasma is equal to that of the bulk solution and that the instrument response function for Cs is the same for the two sample introduction approaches. If q_{plasma} of the sample determined with Cs is representative for analyte NPs, PNC calculation is straightforward, as shown in eqn (10).

$$S_{drop,i} = \frac{I_{drop,i}}{C_{drop,i} \times V_{drop}} \quad (4)$$

$$m_{p,i} = \frac{I_{p,i}}{S_{drop,i}} \quad (5)$$

$$d_{eff,i} = \left(\frac{6m_{p,i}}{\pi\rho_i}\right)^{1/3} \quad (6)$$

$$S_{neb,Cs} = \frac{\lambda_{Neb,Cs}}{C_{Neb,Cs}} \quad (7)$$

$$S_{drop,Cs} = \frac{\left(I_{drop,Cs} - I_{Neb,Cs}\right)}{C_{drop,Cs} \times V_{drop}} \quad (8)$$

$$q_{plasma} = \frac{S_{Neb,Cs}}{S_{drop,Cs}} \quad (9)$$

$$PNC = \frac{f_{NP}}{q_{plasma}} \quad (10)$$

Results and discussion

Online microdroplet calibration with online plasma-uptake measurement offers the possibility to provide accurate NP quantification, both in terms of $m_{p,i}$ and PNC, irrespective of the sample matrix. Importantly, the use of a plasma-uptake standard in both microdroplets and in the NP-containing matrix allows for the separation of plasma-related and sample-introduction-related matrix effects. The plasma-uptake standard differs from a conventional internal standard[35] because it is only used to correct for uptake into the plasma. As we have previously reported,[30,31] online addition of microdroplet standards compensates for plasma-related matrix effects because both microdroplet standards and analyte NPs experience the same steady state plasma conditions. However, use of microdroplets to calibrate $m_{p,i}$ does not compensate for matrix effects or experimental variability that alter q_{plasma} (and thus the PNC).

Generally, any matrix that changes solution properties such as viscosity, volatility, or surface tension can also affect transport efficiency (η_{neb}) and q_{plasma} because solution properties control droplet size distribution of both the primary aerosol generated by the nebulizer[36] and the secondary aerosol that exits the spray chamber.[37] In conventional particle-size based NP calibrations, a mismatch of η_{neb} between analyte calibration solutions and NP standard suspensions could lead to inaccurate determination of η_{neb} and a systematic error for calibration of analyte NPs.[22] In our setup, the plasma-uptake standard (*i.e.* Cs) present in the microdroplets is automatically matrix matched, and thus $S_{Cs,drop}$ represents a matrix-dependent mass sensitivity. Assuming that signals from microdroplets and nebulized samples experience identical (or very similar) signal attenuation or enhancement in the ICP and MS interface, the determination of q_{plasma} (see eqn (9)) depends only on variability of plasma uptake due to matrix composition or nebulization stability. Moreover, the usefulness of this experimental q_{plasma} for determination of PNC depends on the similarity of the uptake of the dissolved plasma-uptake standard and analyte NPs. In the sections below, we investigate the trueness of these assumptions for online determination of q_{plasma} and its utility for sp-ICP-TOFMS.

Choice of plasma-uptake standard

Selection of the plasma-uptake standard depended on several initial criteria, including low background concentration in analyte matrices of interest (*e.g.* aquatic environmental sample), solubility in matrices of interest, and limited or no interferences with isotopes from analyte NPs. Our first list of plasma-uptake standards included Th, Lu, Ho, and Cs.

However, of these candidates, only Cs remained fully dissolved in neutral water. ICP-TOFMS time traces of $^{133}Cs^{+}$ and $^{165}Ho^{+}$ in DI water and in 1% HNO_3 are provided in Fig. S1.† In addition to complete solubility, we measured a background of 0.01 ng mL^{-1} Cs in water from a local river (Limmat River, Zurich, Switzerland), which is 100-times lower than the 1 ng mL^{-1} final concentration of Cs that we used for online plasma-uptake experiments. At a final Cs concentration of 1 ng mL^{-1}, the concentration of salt due to the addition of Cs^{+} is negligible compared to background salt content, which is in the μg g^{-1} to percent range for most environmental samples. The small contribution of Cs to total ionic strength of the solution should not affect NP stability. To verify that q_{plasma} obtained with Cs as the plasma-uptake standard sufficiently describes plasma uptake for a range of analyte elements, we measured q_{plasma} for several elements in a multi-elemental solution introduced to the ICP coincident with analyte-doped microdroplets. In all cases, q_{plasma} determined with Cs is within 20% of element-specific q_{plasma} values; results are presented in Fig. S2.†

NP-mass and particle-number concentrations in test matrices

To explore the utility of online microdroplet and plasma-uptake calibration, we spiked Au NPs (100 nm nominal diameter) into two challenging matrices, namely phosphate-buffered saline (PBS) and Triton X-114, and then measured recovery in terms of $m_{p,i}$ and PNC. PBS is a typical media for biological samples (cell, protein, DNA, *etc.*) and its high salt concentration is known to attenuate the sensitivity of target elements.[31] Triton is a non-ionic polyoxyethylene surfactant that is sometimes used in procedures to extract NPs.[38] Because Triton and other surfactants alter a sample's physical parameters such as viscosity and surface tension,[35] it could affect nebulized droplet formation and thus q_{plasma}. For each matrix, we ran a series of matrix concentrations each spiked with the same nominal concentration of 100-nm Au NPs and 1 ng mL^{-1} Cs. Results from these experiments are presented for the PBS matrix in Fig. 2. In Fig. S3,† we provide similar results for studies with the Triton X-114 matrix and discuss the results.

As seen in Fig. 2a, the $^{197}Au^{+}$ signal from both microdroplets and NPs is over 2-times lower in the most concentrated PBS solution compared to water. However, in Fig. 2b we demonstrate accurate Au NP diameter measurements in all PBS dilutions. In Fig. 2c, we plot the normalized sensitivities for Cs from both nebulized samples and microdroplets. Compared to Au-signal attenuation in PBS, Cs signal from droplets is attenuated much less and has a different general trend: for Cs, a low concentration of PBS actually causes an enhancement followed by minor attenuation (~20% in the most concentrated PBS solution). Cs signal from the nebulized sample is enhanced much more (up to 100%) than signal from the microdroplets, which indicates that the amount of Cs into the plasma increases with PBS concentration. To

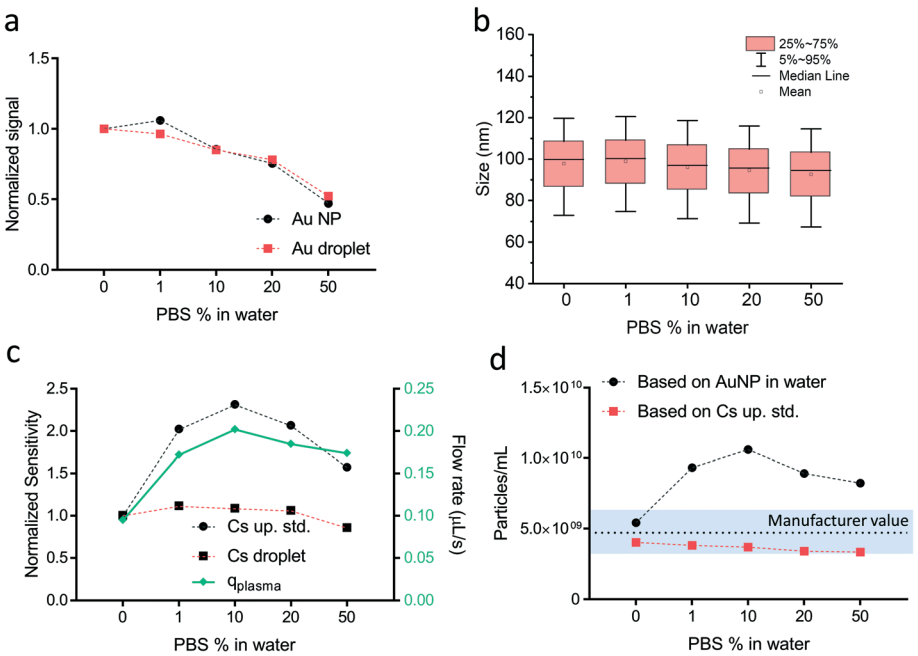

Fig. 2 Study on the effect of the PBS matrix on the calibration NP diameter and PNC. a) Normalized signal intensities from Au in droplets and in NPs for increasing concentrations of PBS. b) Determined Au NP diameters in all PBS solutions. The box and whiskers represent the spread of NP diameters determined in three measurement replicates, each of 150 s in duration. c) Sensitivities for Cs from both nebulized sample and microdroplets normalized to sensitivity values from DI water as a function of PBS concentration with corresponding q_{plasma} values. d) Particle number concentrations of Au NPs based on the conventional particle-size calibration method (black) and online plasma-uptake determination (red).

confirm this, we also measured liquid uptake rate into the nebulizer (see Fig. S4†) during these experiments and observed no change in flow rate with PBS concentration, so increased nebulized-Cs signal is a result of a PBS-concentration-dependent nebulization efficiency. Without plasma-uptake calibration, we could not have discovered that PBS—in addition to causing plasma-related matrix effects—also alters the uptake of sample into the plasma and thus introduces a sample-introduction related matrix effect. In Fig. 2d, we plot PNCs measured assuming a constant transport efficiency as determined with the conventional particle-size method[19] compared to PNCs determined with our online plasma-uptake measurements. As shown, online calibration of plasma uptake reduces overall deviation from the "true" PNC from 100% to <30%, and produces generally more consistent PNC values, with an RSD of 7.9%. It worth mentioning here that the PNC given by the manufacturer is considered as the reference value; this value is an approximation and should not be equated with PNC of a well-characterized NP reference material. Nonetheless, it is evident from comparing the shape experimental q_{plasma} curve with that of the uncorrected PNCs, that online plasma-uptake determination compensates for changes in sample volume introduced into the plasma. Though we can identify, and mostly correct for, both matrix-caused signal attenuation and plasma-uptake variability, we also observe minor mismatch between matrix effects on nanoparticle- and microdroplet-based signals (see Fig. 2a). This mismatch is likely due to slight differences in the vaporization and ionization positions of nebulized aerosols and dried-microdroplet residues in the ICP.[39] More experiments are required confirm this hypothesis.

Multiplexed-NP analysis by sp-ICP-TOFMS

As demonstrated in the previous section, online microdroplet calibration and online determination of q_{plasma} allow accurate measurement of Au NPs in various challenging matrices. However, a key advantage of our measurement system is the ability to perform simultaneous quantification of multiple NP types. Here, we measured a clean DI water sample and a sample from the effluent of a WWTP in Dübendorf, Switzerland, and spiked each with three commercially available metal nanoparticles, *i.e.* Ag, Pt, and Au NPs. For this study, we doped microdroplet standards with 50 ng mL^{-1} of five elements: Ag, Cs, Ce, Pt and Au. In addition, we spiked Cs (the plasma-uptake standard) into the DI water and WWTP effluent at a final concentration of 1 ng mL^{-1}. NPs from the WWTP effluent sample were measured as close to *in situ* as possible, without any addition of surfactants for NP stabilization or sonication treatment. Quantification of NPs was performed *via* online microdroplet calibration with no external NP standards and no measurement of sample flow rate into the nebulizer.

Results from online calibration of NP-diameter ($d_{eff,i,NP}$) and PNC for spiked NPs into the WWTP effluent are provided in Fig. 3. To verify the manufacturer-reported NP diameters, we performed scanning electronic microscopy (SEM) analysis of the stock NP suspensions and analyzed the images using ImageJ Software embedded particle analysis feature,[40] see

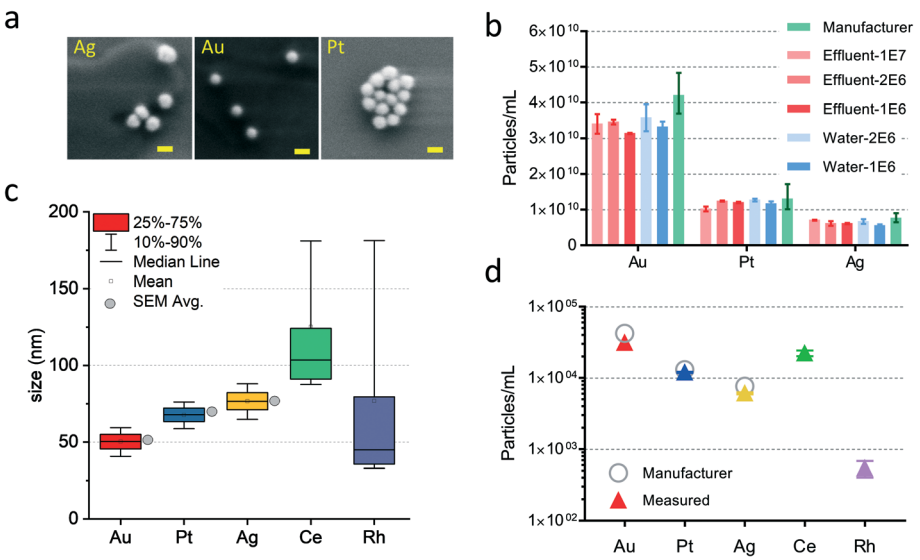

Fig. 3 a) Scanning electron microscopy images of spiked nanoparticles (scale bars are 100 nm). b) Stock PNCs measured by sp-ICP-TOFMS. Mixtures of three synthetic nanoparticle types (Au, Pt, and Ag) were analyzed at several dilutions (dilution factor listed in key) in both DI water and waste water treatment plant (WWTP) effluent. Simultaneous diameter (c) and PNC (d) determination of the spiked NPs (Au, Pt, and Ag) into the WWTP effluent match manufacturer specifications. In addition, several endogenous NP types (including cerium- and rhodium-containing NPs) were found in the WWTP effluent; determined effective diameters and PNC values of these particles are provided. In b and d, the error bars are ±1σ (standard deviation) from three replicate measurements, each of 150 s in duration. The box and whiskers in c represent the spread of NP diameters determined in all three measurement replicates.

Fig. S5.† The median sizes value obtained from SEM are in agreement with the manufacturer data but the standard deviation for our measurement is high due to the relatively small sample size: only ~100 particles per SEM size distribution. Furthermore, silver NPs—which are sensitive particle to light[21]—show a wider distribution tail toward smaller NP diameter; this is evidence for degradation of the NPs (see Fig. S5e†).

In Fig. 3b, we report the back-calculated PNCs measured from several different NP spike concentrations in water and the WWTP effluent. We observe no difference (within experimental uncertainty) between PNC in water or WWTP effluent. However, we do observe that, while the PNCs for Pt and Ag are within the expected concentration range (*i.e.* within uncertainty of the manufacturer-reported NP concentrations), the Au NP PNC is consistently lower than expected. This low Au PNC is likely due to the presence of some particle events below the detectable level: the average $^{197}Au^{+}$ signal per 50 nm Au NP was only ~15 counts in our experiments.

In Fig. 3c and d, we plot $d_{eff,i}$ and PNC values of both spiked engineered NPs (*i.e.* Au, Pt, and Ag) and endogenous particles present in the WWTP effluent sample. All NP signals were found by fitting *m*/*z*-specific background signals with a compound Poisson distribution[32,34] and then thresholding ICP-TOFMS data at a critical value (S_C) that predicts 0.01% false-positive particle signals. As seen, the determined $d_{eff,i}$, and PNC values of the spiked engineered NPs match well with expectation. In addition to measuring ICP-TOFMS signals from the spiked NPs, the whole elemental mass spectrum of the WWTP effluent sample was analyzed using in-house software developed for multiplexed nanoparticle analysis. In Fig. 3c we plot the effective diameters of the Ce-containing NPs, assuming chemical composition and density of CeO_2 and Rh metal. Importantly, $d_{eff,i}$ of these found NPs is probably not indicative of actual NP size, because some elements, such as Rh, were present in multi-element NPs, and no particle shape information is known. While only Ce- and Rh-containing NPs are reported in Fig. 4, particles composed of Ti, Cr, Fe, Mn, Cu, Sn, La, Pr, and Pb were all also found in the WWTP effluent. The PNCs of all these measured NP types, as well as the mass fractions of analyte NPs in the WWTP effluent are reported in Table S2.† In Fig. S6,† we provide the average mass spectrum from 10 Rh-containing NP signals, which confirms that $^{103}Rh^{+}$ signals originate from Rh and is not the result of a spectroscopic interference, such as from $^{63}Cu^{40}Ar^{+}$, $^{23}Na^{40}Ar_2{}^{+}$, $^{87}SrO^{+}$, or $^{206}Pb^{2+}$.

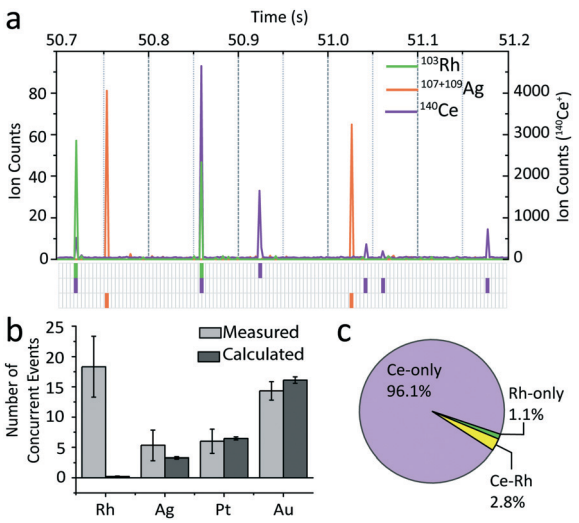

Fig. 4 (a) A 500-ms section of sp-ICP-TOFMS time trace of WWTP effluent with spiked Ag, Pt, and Au NPs. Only ^{103}Rh, $^{107+109}Ag$ and ^{140}Ce signals shown. Some concurrent single-particle signals are random, but others are due to true multi-element composition of the particles. The colored bars directly below the time trace show which signals are identified as particles. (b) Predicted *vs.* measured number of concurrent NP events with Ce-NPs; the error bars represent $\pm 1\sigma$ (standard deviation) from three replicate measurements, each of 150 s in duration. Rh is concurrent with Ce much more often than predicted, which indicates a Rh–Ce NP sub-class of Ce NPs. (c) Ce and Rh NPs in WWTP effluent; at least two NP types are present: likely CeO_2 and Rh–CeO_2 NPs. The Rh-only NPs may have Ce content below detectable levels or represent a third class of particles.

To determine whether coincident NP events were statistically likely to be from a single source (*i.e.* in a single particle) or from independent sources (*i.e.* two particles that happen to be in the plasma at the same time), we performed a simple event concurrency analysis. In this analysis, we assume that all NP signals are from independent particles and that the probability (**P**) of measuring a single analyte NP, $\mathbf{P}(NP_i)$, is the number of NPs of that analyte divided by the total number of time points in a given measurement. The probability that two independent NPs are measured at the same time is the product of the two independent probabilities, $\mathbf{P}(NP_a \cap NP_b)$.

In Fig. 4, we plot the predicted number of coincident particle events of Rh, Ag, Pt, and Au NPs with Ce NPs. As seen, the predicted number of coincident particle events for Ag, Pt, and Au with Ce match the number of multi-element NP events measured, which confirms that the Ag, Pt, Au, and Ce NPs are all independent of one another. However, the number of measured Rh–Ce coincident single-particle events greatly outnumbers the prediction; this indicates that there is a sub-class of CeO_2 NPs that also contain Rh. The origin of these Rh–CeO_2 NPs is still under investigation; however, the unique combination of Rh and Ce suggests that the particles originate from CeO_2-supported platinum-group metal (PGM) catalysts; such PGM-CeO_2 catalysts are widely applied in automobile catalytic converters and in other industrial applications.[41,42] Of note, we did not find other PGM (*e.g.* Pd, Pt, or Ir) single particles in the WWTP effluent, either associated with Ce or not. Additionally, we found no association of Ce NPs with other elements, such as La, Pr, or Th, that could indicate presence of naturally occurring Ce-containing NPs.[10,12,20,43] Our results indicate that multi-element fingerprinting by sp-ICP-TOFMS offers the possibility to distinguish—on a single-particle level—Ce-containing NPs due catalytic applications from those due to other sources, such as from glass polishing industries,[44,45] other engineered CeO_2

NPs,[46] or natural Ce-containing nanoclays.[10,12] Multi-element fingerprinting provides a means to discover, identify, and quantify NP sub-classes, and, together with multi-isotope fingerprinting, is an emerging area of research in environmental nanoparticle analysis.[10,18,47,48] With multi-elemental sp-ICP-TOFMS, event concurrency analysis is a straightforward approach to identify multi-element correlations even within sub-populations of a given NP type and is especially well-suited to identification of low-abundance multi-element NPs.

Conclusions

We demonstrated that online microdroplet calibration with online plasma-uptake determination allows for simultaneous matrix-matched quantification of diverse metal-containing NPs in terms of both element mass and particle number concentration. This quantification is achieved without external NP standards or measurement of sample introduction rates into the nebulizer, which improves sp-ICP-MS analysis throughput. Our method relies on online mixing of microdroplet standards with nebulized NP-containing samples that are spiked with a plasma-uptake standard (*e.g.* Cs). Because sensitivity from microdroplets are matrix dependent, sample uptake measured with nebulized Cs signal is independent of plasma-related matrix effects and is a direct measure of sample-introduction effects. Online microdroplet calibration with full-spectrum measurement provided by ICP-TOFMS allows for high-throughput, multiplexed NP analysis; however, this calibration method, in principle, could also be applied to sp-ICP-MS with quadrupole or sector-field mass analyzers. Further automation of our method for higher sample throughput could also be achieved with online mixing of the plasma-uptake standard and NP-containing samples, such as with a multi-spray nebulizer.[49]

Matrix-matched calibration of diverse NPs makes our sp-ICP-TOFMS methods especially well-suited for the *in situ* analysis of engineered and incidental nanomaterials in challenging matrices such as in biological samples or high-salt-content environmental samples. Our approach should also be directly applicable for metals analysis of single cells. Through the analysis of WWTP effluent, we demonstrated how our approach can be used for the simultaneous quantification of spiked engineered NPs and endogenous NPs likely of anthropogenic origin. A simple event concurrency analysis allowed us to recognize that Ce-NP signals were divided between into two distinct particle classes: Ce-only NPs that are likely engineered CeO_2 NPs and particles we tentatively identified as Rh–CeO_2 NPs that are present at roughly two orders of magnitude lower PNC than the CeO_2 particles. Importantly, the use of ICP-TOFMS with simultaneous full-spectrum detection allows for the untargeted measurement of NP mixtures and discovery of unique multi-element NP species. The WWTP effluent sample we examined had high concentration of Ce particles and unique particles with multi-element signatures of Rh and Ce; however, sp-ICP-TOFMS with online microdroplet calibration is also well suited for NP quantification and multi-element characterization of other particle types. Future research is required to verify our Ce-NP classification; however, our findings support the continued investigation and potential discriminatory power of multi-element fingerprinting to source and classify Ce NPs.

Conflicts of interest

There are no conflicts of interest to declare.

Acknowledgements

The authors wish to thank Dr. Alexander Gogos and Dr. Ralf Kägi from Eawag (Dübendorf, Switzerland) for collection of the WWTP effluent samples. The authors thank Roland Mäder from the ETH mechanical workshop for manufacturing components of the dual sample introduction setup. A G.-G. and K.M.K. acknowledge funding through an Ambizione grant of the SNSF, project no. PZ00P2_174061.

References

1 J. Scott-Fordsmand, W. Peijnenburg, E. Semenzin, B. Nowack, N. Hunt, D. Hristozov, A. Marcomini, M. A. Irfan, A. S. Jiménez and R. Landsiedel, Environmental risk assessment strategy for nanomaterials, *Int. J. Environ. Res. Public Health*, 2017, **14**, 1251.

2 D. M. Mitrano, K. Mehrabi, Y. A. R. Dasilva and B. Nowack, Mobility of metallic (nano) particles in leachates from landfills containing waste incineration residues, *Environ. Sci.: Nano*, 2017, **4**, 480–492.

3 M. Bundschuh, J. Filser, S. Lüderwald, M. S. McKee, G. Metreveli, G. E. Schaumann, R. Schulz and S. Wagner, Nanoparticles in the environment: where do we come from, where do we go to?, *Environ. Sci. Eur.*, 2018, **30**, 6.

4 M. F. Hochella, D. W. Mogk, J. Ranville, I. C. Allen, G. W. Luther, L. C. Marr, B. P. McGrail, M. Murayama, N. P. Qafoku, K. M. Rosso, N. Sahai, P. A. Schroeder, P. Vikesland, P. Westerhoff and Y. Yang, Natural, incidental, and engineered nanomaterials and their impacts on the Earth system, *Science*, 2019, **363**(6434), eaau8299.

5 P. Westerhoff, A. Atkinson, J. Fortner, M. S. Wong, J. Zimmerman, J. Gardea-Torresdey, J. Ranville and P. Herckes, Low risk posed by engineered and incidental nanoparticles in drinking water, *Nat. Nanotechnol.*, 2018, **13**, 661–669.

6 B. Giese, F. Klaessig, B. Park, R. Kaegi, M. Steinfeldt, H. Wigger, A. von Gleich and F. Gottschalk, Risks, release and concentrations of engineered nanomaterial in the environment, *Sci. Rep.*, 2018, **8**, 1565.

7 F. Laborda, E. Bolea, G. Cepriá, M. T. Gómez, M. S. Jiménez, J. Pérez-Arantegui and J. R. Castillo, Detection, characterization and quantification of inorganic engineered nanomaterials: A review of techniques and methodological approaches for the analysis of complex samples, *Anal. Chim. Acta*, 2016, **904**, 10–32.

8 O. Borovinskaya, B. Hattendorf, M. Tanner, S. Gschwind and D. Gunther, A prototype of a new inductively coupled plasma time-of-flight mass spectrometer providing temporally resolved, multi-element detection of short signals generated by single particles and droplets, *J. Anal. At. Spectrom.*, 2013, **28**, 226–233.

9 O. Borovinskaya, S. Gschwind, B. Hattendorf, M. Tanner and D. Günther, Simultaneous Mass Quantification of Nanoparticles of Different Composition in a Mixture by Microdroplet Generator-ICPTOFMS, *Anal. Chem.*, 2014, **86**, 8142–8148.

10 A. Praetorius, A. Gundlach-Graham, E. Goldberg, W. Fabienke, J. Navratilova, A. Gondikas, R. Kaegi, D. Günther, T. Hofmann and F. von der Kammer, Single-particle multi-element fingerprinting (spMEF) using inductively-coupled plasma time-of-flight mass spectrometry (ICP-TOFMS) to identify engineered nanoparticles against the elevated natural background in soils, *Environ. Sci.: Nano*, 2017, **4**, 307–314.

11 S. Naasz, S. Weigel, O. Borovinskaya, A. Serva, C. Cascio, A. K. Undas, F. C. Simeone, H. J. P. Marvin and R. J. B. Peters, Multi-element analysis of single nanoparticles by ICP-MS using quadrupole and time-of-flight technologies, *J. Anal. At. Spectrom.*, 2018, **33**, 835–845.

12 F. von der Kammer, P. L. Ferguson, P. A. Holden, A. Masion, K. R. Rogers, S. J. Klaine, A. A. Koelmans, N. Horne and J. M. Unrine, Analysis of engineered nanomaterials in complex matrices (environment and biota): General considerations and conceptual case studies, *Environ. Toxicol. Chem.*, 2012, **31**, 32–49.

13 N. C. Mueller and B. Nowack, Exposure Modeling of Engineered Nanoparticles in the Environment, *Environ. Sci. Technol.*, 2008, **42**, 4447–4453.

14 R. Handy, F. von der Kammer, J. Lead, M. Hassellöv, R. Owen and M. Crane, The ecotoxicology and chemistry of manufactured nanoparticles, *Ecotoxicology*, 2008, **17**, 287–314.

15 S. J. Klaine, A. A. Koelmans, N. Horne, S. Carley, R. D. Handy, L. Kapustka, B. Nowack and F. von der Kammer, Paradigms to assess the environmental impact of manufactured nanomaterials, *Environ. Toxicol. Chem.*, 2012, **31**, 3–14.

16 B. Nowack, A. Boldrin, A. Caballero, S. F. Hansen, F. Gottschalk, L. Heggelund, M. Hennig, A. Mackevica, H. Maes, J. Navratilova, N. Neubauer, R. Peters, J. Rose, A. Schäffer, L. Scifo, S. v. Leeuwen, F. von der Kammer, W. Wohlleben, A. Wyrwoll and D. Hristozov, Meeting the Needs for Released Nanomaterials Required for Further Testing—The SUN Approach, *Environ. Sci. Technol.*, 2016, **50**, 2747–2753.

17 M. Zhang, J. Yang, Z. Cai, Y. Feng, Y. Wang, D. Zhang and X. Pan, Detection of engineered nanoparticles in aquatic environments: current status and challenges in enrichment, separation, and analysis, *Environ. Sci.: Nano*, 2019, **6**, 709–735.

18 F. Loosli, J. Wang, S. Rothenberg, M. Bizimis, C. Winkler, O. Borovinskaya, L. Flamigni and M. Baalousha, Sewage spills are a major source of titanium dioxide engineered (nano)-particle release into the environment, *Environ. Sci.: Nano*, 2019, **6**, 763–777.

19 H. E. Pace, N. J. Rogers, C. Jarolimek, V. A. Coleman, C. P. Higgins and J. F. Ranville, Determining Transport Efficiency for the Purpose of Counting and Sizing Nanoparticles via Single Particle Inductively Coupled Plasma Mass Spectrometry, *Anal. Chem.*, 2011, **83**, 9361–9369.

20 M. D. Montaño, H. R. Badiei, S. Bazargan and J. F. Ranville, Improvements in the detection and characterization of engineered nanoparticles using spICP-MS with microsecond dwell times, *Environ. Sci.: Nano*, 2014, **1**, 338–346.

21 J. Liu, K. E. Murphy, M. R. Winchester and V. A. Hackley, Overcoming challenges in single particle inductively coupled plasma mass spectrometry measurement of silver nanoparticles, *Anal. Bioanal. Chem.*, 2017, **409**, 6027–6039.

22 M. D. Montaño, J. W. Olesik, A. G. Barber, K. Challis and J. F. Ranville, Single Particle ICP-MS: Advances toward routine analysis of nanomaterials, *Anal. Bioanal. Chem.*, 2016, **408**, 5053–5074.

23 A. Murtazin, S. Groh and K. Niemax, Measurement of element mass distributions in particle ensembles applying ICP-OES, *J. Anal. At. Spectrom.*, 2010, **25**, 1395–1401.

24 S. Gschwind, L. Flamigni, J. Koch, O. Borovinskaya, S. Groh, K. Niemax and D. Gunther, Capabilities of inductively coupled plasma mass spectrometry for the detection of nanoparticles carried by monodisperse microdroplets, *J. Anal. At. Spectrom.*, 2011, **26**, 1166–1174.

25 J. Koch, L. Flamigni, S. Gschwind, S. Allner, H. Longerich and D. Gunther, Accelerated evaporation of microdroplets at ambient conditions for the on-line analysis of nanoparticles by inductively-coupled plasma mass spectrometry, *J. Anal. At. Spectrom.*, 2013, **28**, 1707–1717.

26 L. Telgmann, C. Metcalfe and H. Hintelmann, Rapid size characterization of silver nanoparticles by single particle ICP-MS and isotope dilution, *J. Anal. At. Spectrom.*, 2014, **29**, 1265–1272.

27 H. El Hadri, E. J. Petersen and M. R. Winchester, Impact of and correction for instrument sensitivity drift on nanoparticle size measurements by single-particle ICP-MS, *Anal. Bioanal. Chem.*, 2016, **408**, 5099–5108.

28 M. Á. Aguirre, L. L. Fialho, J. A. Nóbrega, M. Hidalgo and A. Canals, Compensation of inorganic acid interferences in ICP-OES and ICP-MS using a Flow Blurring® multinebulizer, *J. Anal. At. Spectrom.*, 2014, **29**, 1218–1227.

29 B. Ramkorun-Schmidt, S. A. Pergantis, D. Esteban-Fernández, N. Jakubowski and D. Günther, Investigation of a Combined Microdroplet Generator and Pneumatic Nebulization System for Quantitative Determination of Metal-Containing Nanoparticles Using ICPMS, *Anal. Chem.*, 2015, **87**, 8687–8694.

30 L. Hendriks, A. Gundlach-Graham and D. Günther, Analysis of Inorganic Nanoparticles by Single-Particle Inductively Coupled Plasma Time-of-Flight Mass Spectrometry, *Chimia*, 2018, **72**, 221–226.

31 L. Hendriks, B. Ramkorun-Schmidt, A. Gundlach-Graham, J. Koch, R. N. Grass, N. Jakubowski and D. Günther, Single-particle ICP-MS with online microdroplet calibration: toward matrix independent nanoparticle sizing, *J. Anal. At. Spectrom.*, 2019, **34**, 716–728.

32 A. Gundlach-Graham, L. Hendriks, K. Mehrabi and D. Günther, Monte Carlo Simulation of Low-Count Signals in Time-of-Flight Mass Spectrometry and its Application to Single-Particle Detection, *Anal. Chem.*, 2018, **90**, 11847–11855.
33 M. Burger, L. Hendriks, J. Kaeslin, A. Gundlach-Graham, B. Hattendorf and D. Günther, Characterization of inductively coupled plasma time-of-flight mass spectrometry in combination with collision/reaction cell technology – insights from highly time-resolved measurements, *J. Anal. At. Spectrom.*, 2019, **34**, 135–146.
34 L. Hendriks, A. Gundlach-Graham and D. Günther, Performance of sp-ICP-TOFMS with signal distributions fitted to a compound Poisson model, *J. Anal. At. Spectrom.*, 2019, **34**, 1900–1909.
35 C. Agatemor and D. Beauchemin, Matrix effects in inductively coupled plasma mass spectrometry: a review, *Anal. Chim. Acta*, 2011, **706**, 66–83.
36 B. L. Sharp, Pneumatic nebulisers and spray chambers for inductively coupled plasma spectrometry. A review. Part 1. Nebulisers, *J. Anal. At. Spectrom.*, 1988, **3**, 613–652.
37 B. L. Sharp, Pneumatic nebulisers and spray chambers for inductively coupled plasma spectrometry. A review. Part 2. Spray chambers, *J. Anal. At. Spectrom.*, 1988, **3**, 939–963.
38 H. El Hadri and V. A. Hackley, Investigation of cloud point extraction for the analysis of metallic nanoparticles in a soil matrix, *Environ. Sci.: Nano*, 2017, **4**, 105–116.
39 K. Niemax, Considerations about the detection efficiency in inductively coupled plasma mass spectrometry, *Spectrochim. Acta, Part B*, 2012, **76**, 65–69.
40 C. A. Schneider, W. S. Rasband and K. W. Eliceiri, NIH Image to ImageJ: 25 years of image analysis, *Nat. Methods*, 2012, **9**, 671.
41 K. C. Taylor, Nitric Oxide Catalysis in Automotive Exhaust Systems, *Catal. Rev.: Sci. Eng.*, 1993, **35**, 457–481.
42 A. Trovarelli, C. de Leitenburg, M. Boaro and G. Dolcetti, The utilization of ceria in industrial catalysis, *Catal. Today*, 1999, **50**, 353–367.
43 M. D. Montaño, G. V. Lowry, F. von der Kammer, J. Blue and J. F. Ranville, Current status and future direction for examining engineered nanoparticles in natural systems, *Environ. Chem.*, 2014, **11**, 351–366.
44 T. Hoshino, Y. Kurata, Y. Terasaki and K. Susa, Mechanism of polishing of SiO2 films by CeO2 particles, *J. Non-Cryst. Solids*, 2001, **283**, 129–136.
45 W. Peng, C. Guan and S. Li, Material removal mechanism of ceria particles with different sizes in glass polishing, *Opt. Eng.*, 2014, **53**, 035104.
46 F. Gómez-Rivera, J. A. Field, D. Brown and R. Sierra-Alvarez, Fate of cerium dioxide (CeO2) nanoparticles in municipal wastewater during activated sludge treatment, *Bioresour. Technol.*, 2012, **108**, 300–304.
47 A. Gondikas, F. von der Kammer, R. Kaegi, O. Borovinskaya, E. Neubauer, J. Navratilova, A. Praetorius, G. Cornelis and T. Hofmann, Where is the nano? Analytical approaches for the detection and quantification of TiO2 engineered nanoparticles in surface waters, *Environ. Sci.: Nano*, 2018, **5**, 313–326.
48 X. Yang, X. Liu, A. Zhang, D. Lu, G. Li, Q. Zhang, Q. Liu and G. Jiang, Distinguishing the sources of silica nanoparticles by dual isotopic fingerprinting and machine learning, *Nat. Commun.*, 2019, **10**, 1620.
49 K. I. Kazumi Inagaki, S.-I. Miyashita, Y. Zhu, T. Ariga, S.-I. Fujii and A. Hokura, *presented in part at the European Winter Conference on Plasma Spectrochemistry*, Pau, France, 2019.

